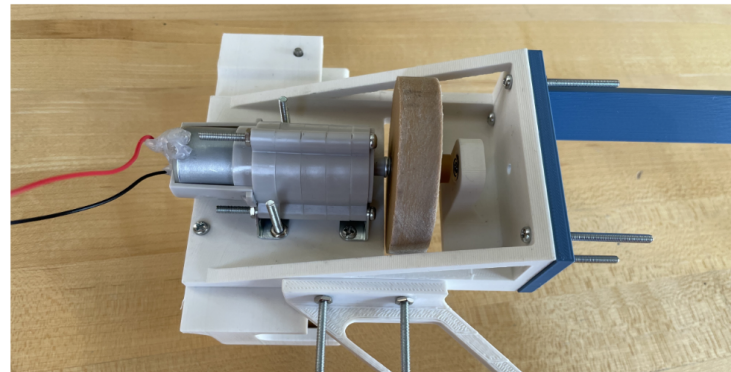
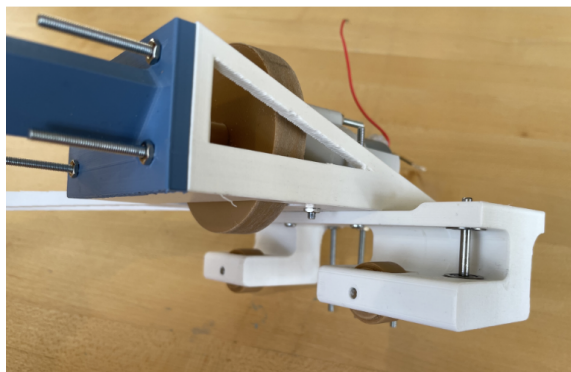
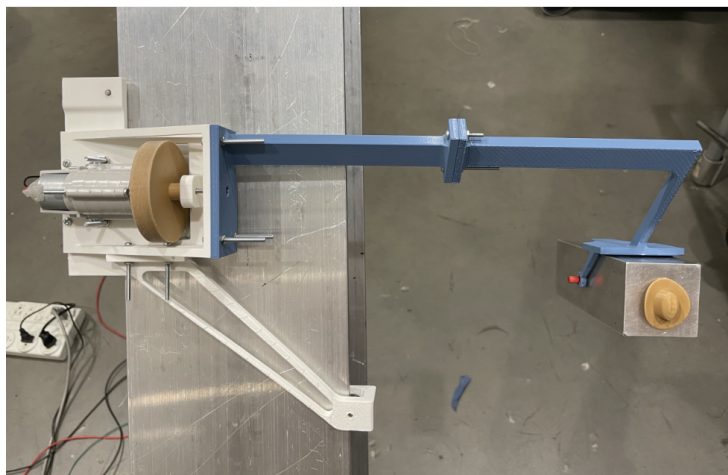
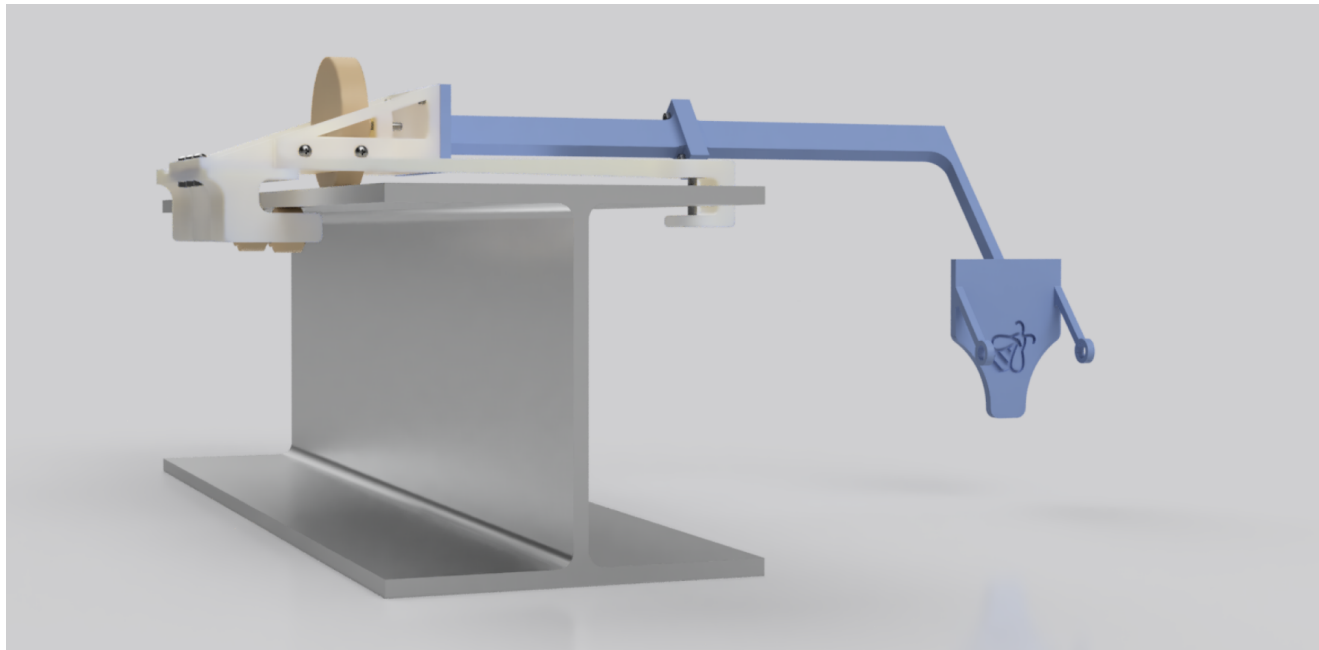


“Going the Distance” Robot



CAD Assembly: <https://a360.co/3Gw8ZTi>

Test Video: <https://drive.google.com/file/d/1u5k1MSxgbYmf6u4M6NyjfDXX6lbgR8lk/view?usp=sharing>

Summary

In order to move one meter up an inclined I-beam as fast as possible while carrying an offset payload, we designed our robot to maximize mechanical power. To do so, we applied 6V, the maximum allowable input voltage, at a set-point of half the maximum motor output torque. We then related the motor's gear efficiencies and known forces to derive the corresponding radius of the drive wheel. All other idle wheels were designed to minimize energy loss by minimizing radii, using bearings, and reducing rolling deformation by designing wheels with sufficient width and printing with high infill. Wheels are simply supported to distribute shaft and bearing loads.

Components are designed for modularity in order to efficiently leverage additive manufacturing. Separate components allowed us to decrease print time, iterate rapidly, and isolate areas of interest in simple sections to localize analysis. We chose a large factor of safety on all of our printed parts to safeguard against manufacturing inconsistencies due to unreliable machinery, resulting in thicker geometry. The orientation of prints were primarily influenced by constraints due to printer bed size, time, and placement of support material rather than prioritizing layer generation in a plane optimal for the loading scenario.

All components attach to the chassis, which houses the motor and driving wheel. Two triangular faces create truss-like tension arms with minimal mass to resist deflection where the cantilever arm attaches. Both the bottom leg and the underside component attach to the left of the driving wheel where deflection is minimal.

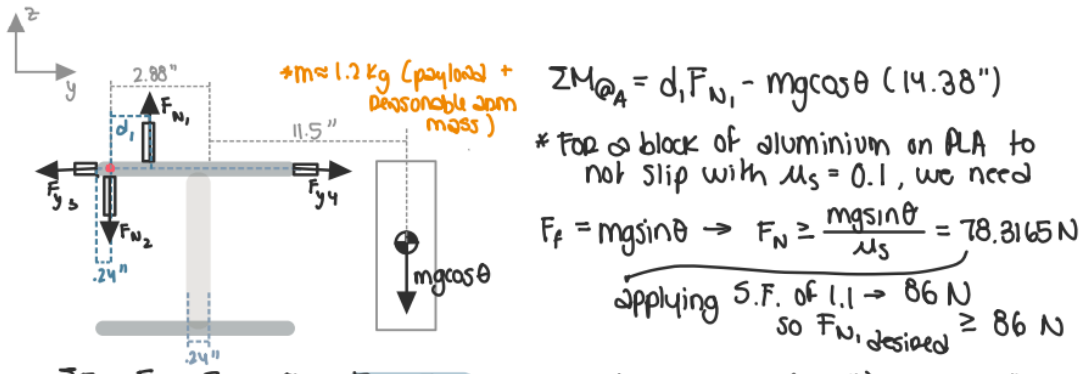
The feature key to our robot's functionality was leveraging the moment created by the payload and cantilever arm; the force from the payload reacted by the driving wheel and the relative distance between the load, the idle wheels on the far left end, and the driving wheel increases the normal force on the driving wheel to prevent slipping. Rotational stability is increased by using two offset wheels on the underside. The cantilever arm is optimized to minimize deflection across its length. This arm is split into two parts due to manufacturing constraints and is connected with bolts and nuts that result in only normal forces at the connecting surfaces and tensile loading on the bolts.

To counteract moments driving the robot off the beam, wheels roll on the left and right lip of the I-beam's top flange. Though we wanted to maximize length between these wheels to minimize their normal force, we also needed to balance mass efficiency, print time, and higher risk of failure with loading longer components. We set the distance for the left lip wheel such that it could be manufactured in the underwheel housing component to reduce hardware usage and complexity. To hold the right wheel, we drew from our experience completing project one to design a mass efficient leg that leveraged tension members arranged to maximize the moment of inertia to minimize mass, bending, and deflection.

Free Body Diagrams

By: Britney Ky, Omar Ramos Escoto

Only drive wheel friction is represented since friction forces from the idle wheels are encompassed in our motor set point analysis. The dynamic coefficient of friction of PLA on aluminum used in calculations was .1. To simplify analysis while still accounting for the mass of the robot, we added 150 grams to the payload to partially represent the robot's distributed mass.



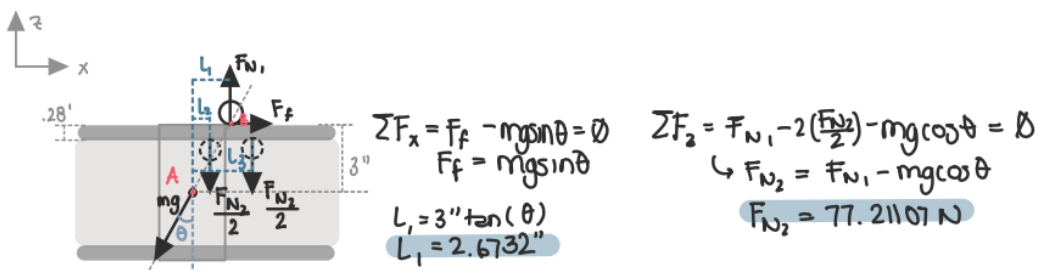
$$\sum F_y = F_{y_3} - F_{y_4} = 0 \rightarrow F_{y_3} = F_{y_4}$$

$$\sum F_z = F_{N_1} - F_{N_2} - mg \cos \theta = 0$$

$$F_{N_1} = F_{N_2} + mg \cos \theta$$

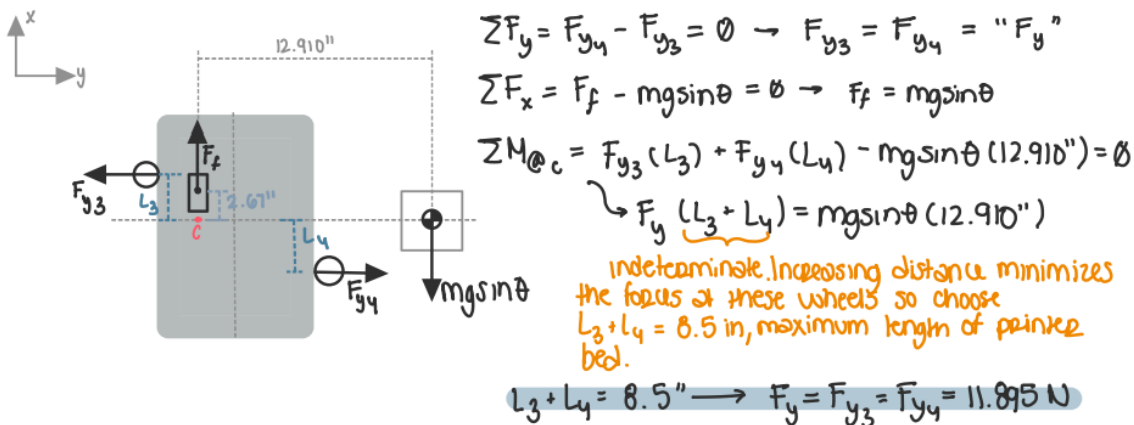
$$L_1 \leq \frac{mg \cos \theta (14.38")}{F_{N_1}} \leq 1.4696"$$

$L_1 = 1.4696"$ to minimize force on underside wheels



$$\begin{aligned} \sum M_{@A} &= F_{N_1} L_1 - F_{N_2}/2(L_2) - F_{N_2}/2(L_3) - F_f(3") = 0 \\ \sum M_{@B} &= mgs \sin \theta (3") - mg \cos \theta (L_1) + F_{N_2}/2(L_1 - L_2) - F_{N_2}/2(L_3 - L_1) = 0 \end{aligned} \quad \left. \begin{array}{l} \text{system solve} \\ \text{for } L_2 \text{ and } L_3 \end{array} \right\}$$

$$\begin{aligned} L_2 &\approx 1.17" \\ L_3 &\approx 4.17" \end{aligned}$$



Transmission Analysis

By: Omar Ramos Escoto

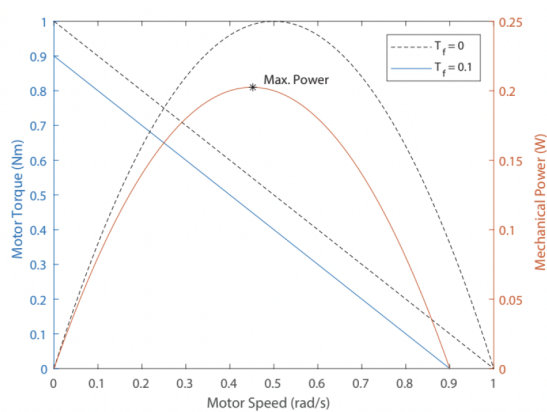
Set-Point Approach:

Travel time is optimized when more work is done per unit time. Using the constant weight of the robot-payload system and climb height, and considering opposing work done by rolling resistance and friction, the work needed to be done by the robot was defined. Since power is work per time, the set-point was guided by maximizing mechanical power by applying the maximum voltage.

Once power was defined in terms of voltage, motor output speed and torque could be determined because maximum mechanical power corresponds to half peak motor speed and half peak motor torque, which were calculated during motor characterization. Therefore, we set the motor output at half peak torque and related it to the torque needed at the driving wheel (the static friction driving force times the driving wheel radius) by using per-stage gear efficiencies and gear ratios, allowing the precise calculation of the driving wheel radius.

The angular velocity of the output—half peak speed at half peak torque—was used to approximate linear velocity. Once the gear configuration and the corresponding wheel radius were set, linear velocity depended on the number of gear stages because adding more stages decreased torque transmission efficiency. For example, when ignoring minute differences between 4:1 and 5:1 gear efficiencies, gear ratios of 64, 80, 100, and 125 with their corresponding wheel radii would result in the same linear velocity since they require 3 gear stages. We ultimately chose a gear ratio based on the wheel radius that would best fit our chassis and motor. We could approximate the motor-to-robot speed ratio since the output wheel rotates at a fraction (gear ratio) of the output shaft of the motor (half peak speed), as speed is not lost to efficiency assuming no slipping occurs.

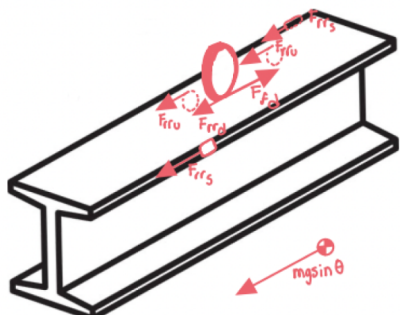
Set-Point Diagrams:



$$P_{max} \approx \frac{1}{4} \cdot \frac{1}{R} \cdot V_{appl}^2$$

$$T_{max} = \frac{1}{2} \cdot \left(\frac{k}{R} \cdot V_{appl} - T_{fric} \right)$$

As discussed previously and seen in the above equations, maximum mechanical power is proportional to applied voltage squared, ignoring friction. Therefore, the voltage was set to be the maximum allowable voltage, 6 Volts. As shown in the graph above, maximum mechanical power corresponds to half peak torque and half peak speed, which became the set point for our motor. This, along with determining the force required to keep the robot moving forward allowed us to determine specific sets of gear ratios and wheel radii to achieve the motor set-point. We chose a gear ratio of 80 and radius of 3.1613 cm to best fit our chassis and motor design. The gear ratio, radius and the half no-load speed can then be used to approximate the motor-to-robot speed ratio.



From FBD's:

$$F_{rrd} = (86 \text{ N})(0.004) = .344 \text{ N}$$

$$F_{rru} = (38.605535 \text{ N})(0.004) = .1544 \text{ N}$$

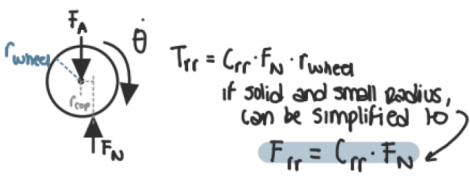
$$F_{rrs} = (11.895 \text{ N})(0.001) = .011895 \text{ N}$$

$$F_{fd} = F_{rrd} + 2F_{rru} + 2F_{rrs} + magin\theta$$

$$F_{fd} = 8.508 \text{ N} \leftarrow \text{achievable since } F_{friction} \leq 8.6 \text{ N.}$$

$$T_{motor} = .5T_{stall} = \frac{F_{fd}r_w}{n_{G}^n R_G} \rightarrow r_w = \frac{.5T_{stall} n_{G}^n R_G}{F_{fd}}$$

where $n_{G} \approx .78$



$C_{rr} \approx .004$ for underside and driving wheel. Conservative estimate between ball bearing (.001) and high-pressure bike tire (.005)

$C_{rr} \approx .001$ conservative, steel on aluminum

Here:	possible R_G	chosen R_G	wheel radius
$n = 0 \rightarrow 0$	0	...	1.01 cm
$n = 1 \rightarrow 4, 5$	4, 5	...	1.267 cm
$n = 2 \rightarrow 16, 20, 25$	16, 20, 25	...	2.529 cm
$n = 3 \rightarrow 64, 80, 100, 125$	64, 80, 100, 125	...	3.1613 cm
		...	3.9517 cm

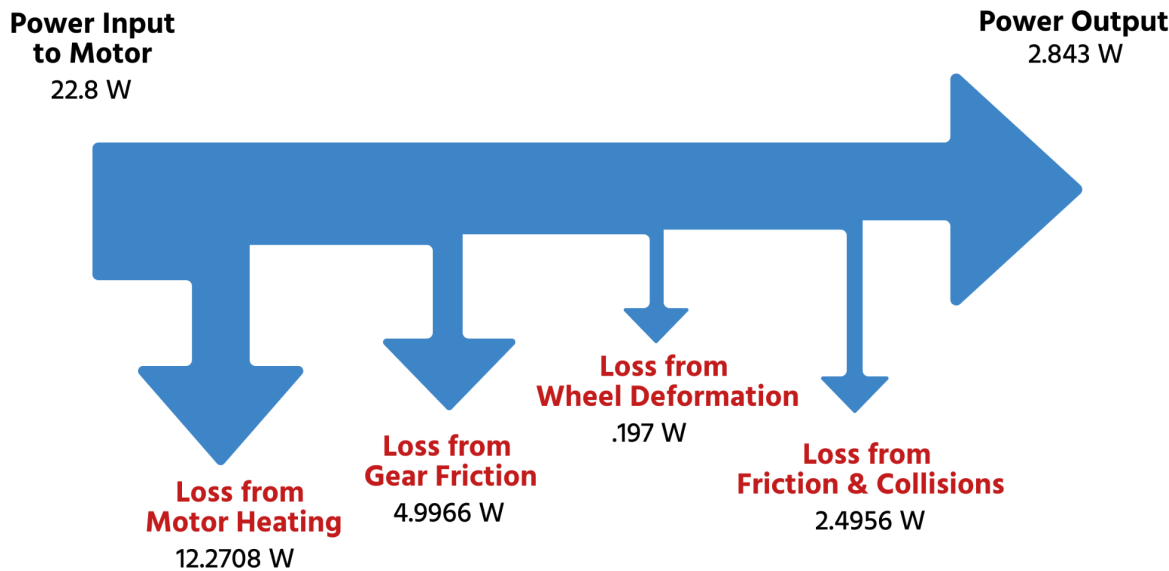
easiest to use since motor front has a radius of around 1.7 cm

$$.5T_{stall} \rightarrow .5\theta_{no load} \approx 1,360 \frac{\text{rad}}{\text{s}}$$

$$v = r\omega = \frac{d}{t} \rightarrow t = \frac{d}{r\omega} = \frac{1\text{m}}{r_w \frac{.5\theta_{no load}}{R_G}}$$

same time for 2 gear stages, around 1.45 sec.
for any 3 gear stage configuration, around 1.85 sec

Energy Flow:



Input: electrical power supplied

$$P_{elec} \approx i_{avg} V_{app} = (3.8 A)(6.0 V)$$

$$P_{elec} = 22.8 W$$

Losses: Joule motor heating (armature and brush contact losses)

Voltage drop due to motor resistance

$$P_{arm} = i_{arm}^2 R_{arm} \quad \text{and} \quad R_{arm} \approx R_{motor}$$

$$= (3.8 A)^2 (0.849780 \Omega \text{ms})$$

$$P_{arm} = 12.2708 W$$

Losses: Gear friction heating

* Assuming that gear efficiency encompasses all energy losses

$$\frac{n_{4:1}}{n_{5:1}} \approx 80\% \quad \left. \right\} \text{ approx } 78\% \text{ per stage from characterization}$$

$$P_{into \ gears} = P_{elec} - P_{arm} = 10.52917 W$$

$$P_{gears} = n_4^3 (10.52917 W)$$

$$P_{gears} = 4.9966 W$$

Losses: Collisions

* Assumed to be negligible because we examined beam to find a 1m section with no bumps that would be big enough (compared to wheel radii) to cause negligible collisions

$$P_{collisions} \approx 0 W$$

Losses: wheel deformation:

$$\text{From free body diagram: } F_{rrd} = (86 N)(0.004) = .344 N$$

$$F_{rru} = (38.605535 N)(0.004) = .1544 N$$

$$F_{rrs} = (11.895 N)(0.001) = .011895 N$$

$$\begin{aligned} r_{side} &= .0014605 m & T_{rrs} &= F_{rrs} \cdot r_s = 1.7372 \times 10^{-5} N \cdot m \\ r_{under} &= .01 m & T_{rru} &= F_{rru} \cdot r_u = 0.001544 N \cdot m \\ r_{driving} &= .031316 m & T_{rrd} &= F_{rrd} \cdot r_d = 0.010772704 N \cdot m \end{aligned}$$

Side wheels:

$$\text{revolutions for 1m} = 108.9729 \rightarrow 684.697 \text{ rads/m}$$

Top driving wheel:

$$\text{revolutions for 1m} = 5.08448 \rightarrow 31.6326 \text{ rads/m}$$

Under wheel:

$$\text{revolutions for 1m} = 15.91549 \rightarrow 100 \text{ rads/m}$$

Energy loss per wheel

$$\begin{aligned} \text{side} &= T_{rrs} \cdot 684.697 \cdot 2 = .02379 J & \text{Total energy} \\ \text{top} &= T_{rrd} \cdot 31.6326 = .24077 J & \text{loss } 0.6135 J \\ \text{under} &= T_{rru} \cdot 100 \cdot 2 = .3088 J & \text{over } 3.41 \text{ sec} \\ \therefore P &= 0.197 W \end{aligned}$$

Losses: Friction

$$P_{loss} = F_{fric} \cdot \dot{x}$$

$$F_{fric} = 8.51 N \quad \leftarrow \text{calculated already taking other wheel deformation into account. It is most substantial friction on system}$$

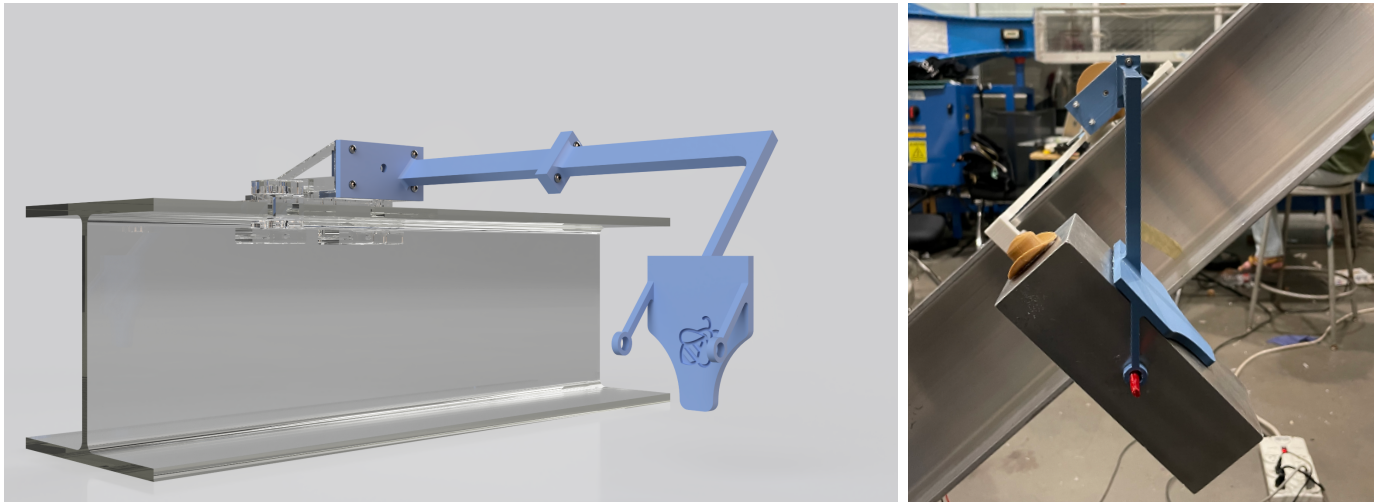
$$P_{frict} = 8.51 N \cdot \left(\frac{1}{3.41} \frac{m}{s} \right)$$

$$P_{frict} = 2.4956 W$$

Component One Analysis

Payload Arm:

By: Hallie Mikacich



Mechanical advantage generated by this component provides a greater normal force essential to preventing slipping. Because the lever arm must extend from the left edge of the I-beam to the payload, our primary concern was minimizing deflection such that the arm would not contact the I-beam or shift significantly, causing energy losses and significantly altering the loading scenario designed for. The arm is oriented such that its midplane is in line with the payload's weight and the driving wheel's point of contact. This orientation is essential to minimizing mass since torsion is eliminated and the only concern becomes the inherent bending moment of a cantilever beam loaded with planar forces. Using solid rectangular geometry minimized volume for printing efficiency and allowed for independent, direct deflection optimization in the respective planes.

The wall that supports the payload extends above and below its centroid to constrain the payload's degrees of freedom as the robot accelerates. All vertical arms are axially loaded in pure tension as they are in line with the payload's weight, eliminating bending moments and thus requiring smaller cross-sectional areas.

Due to printer constraints, the arm was printed in two pieces and is assembled via two nuts and bolts aligned orthogonally to the applied load to minimize shear on the bolts. Thus, only normal contact forces between the bottom of the mating surfaces and tensile loading of the top bolt and nut are present, improving loading and decreasing forces because of the wider spacing of the reaction points. The arm attaches to the chassis with four nuts and bolts to distribute forces amongst more connection points as this is where stress is the highest. The flange contains a hole in the center to provide clearance for a pin that provides simple support to the driving wheel.

BOTEA & Inverse Analysis:

Tension arms (one on each side of payload to prevent sideways motion)

$$F_T = \frac{(1.1 \text{ kg})(9.81 \frac{\text{m}}{\text{s}^2})}{2} = 5.3955 \text{ N}$$

$$\sigma_{\max} = \frac{F}{th} = \frac{S_y}{F_{OS}} \rightarrow th = \frac{F \cdot F_{OS}}{S_y} = \frac{(5.3955 \text{ N})(2)}{(50 \times 10^9 \text{ Pa})} = .0000002158 \text{ m}^2$$

very small,
minimum

$$\omega = .0000464 \text{ m}$$

make $\omega = 4 \text{ mm}$ (10 times of what is needed) because the time and material cost of needing to print again is high. Handling, storing, and testing with acceleration see unknowns that suggest safety factor should be very big in all direction.

Cantilever arm:

- main mode of failure is deflection because excessive deflection will change loading scenario optimized for. Although there is a limit on deflection in the assignment, I will limit it to 5 mm.

$$\delta_{\text{defeat.}} = .005 = \frac{FL^3}{3I} \approx \frac{12(12 \text{ N})(.295 \text{ m})^3}{3(3.6 \times 10^9 \text{ Pa})(bh^3)}$$

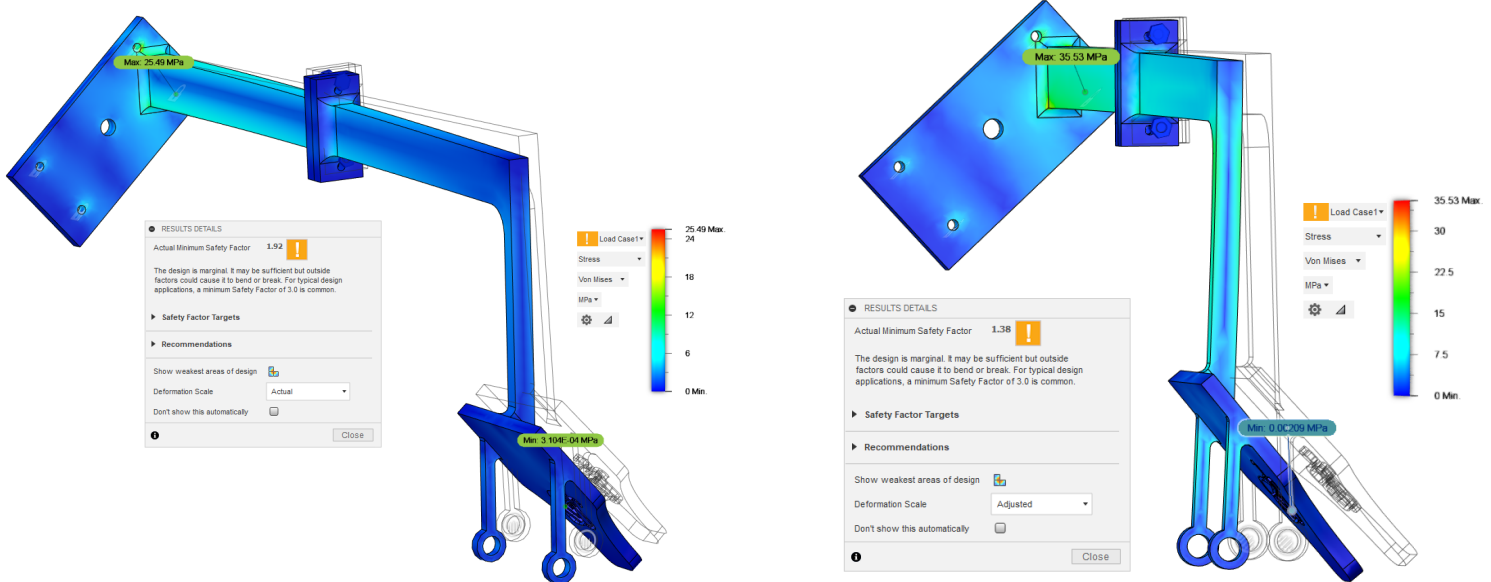
$$bh^3 = 6.85627 \times 10^{-8} \text{ m}$$

- I also want to minimize side-to-side deflection that can occur during acceleration due to the payload's inertia but not as big of a concern as up and down so make $b = \frac{1}{2}h$, only twice as much deflection possible in that plane (1 cm).

$$\left. \begin{aligned} bh^3 &= 6.85627 \times 10^{-8} \text{ m} \\ b &= \frac{1}{2}h \end{aligned} \right\} \quad \begin{aligned} b &= .96 \text{ mm} \\ h &= 1.92 \text{ cm} \end{aligned}$$

* confirmed
not to fail
due to bending
as well

FEA Analysis:



Constraints and Loading:

FEA analysis was conducted for stress and deformation. Fusion360 material libraries do not include PLA, so it was instead modeled with acrylic because the material properties are similar. To simulate interaction with the chassis and bolts, which we considered rigid in order to simplify analysis, the four holes on the attachment flange were fixed to locally constrain all degrees of freedom. The two parts of the arm are connected at the flange with bolt connections. Bolt connections mathematically represent threaded fasteners that hold an assembly together. We also specified a subtype for nut connections to accurately simulate our assembly method. In one loading scenario (left image), a 12N load, the approximate payload weight plus arms' distributed weight, was applied downward on the holes that hold the pin and payload as described in our BOTEAs and FBDs. In another analysis (right image), 12N was applied along the I-beam's axis in the opposite direction of movement to model the inertia of the payload as it accelerates from rest. Bearing loads were used to simulate the parabolic distribution of the force from the pin onto the mounting holes.

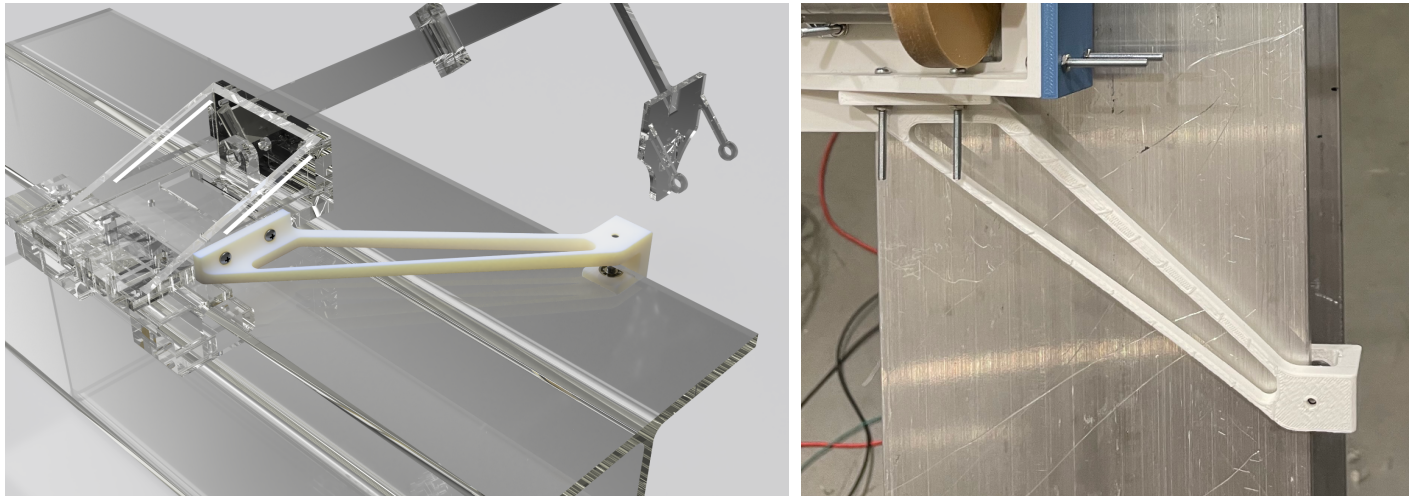
FEA Analysis:

As anticipated, stress patterns indicate that the component is undergoing bending across the horizontal length of the arm. The highest stress concentrations manifest where the wall is fixed to the chassis, expected in any cantilever configuration. When mounted on the I-beam, the end of the arm displays minimal deflection, as indicated by both FEAs which validate our BOTEAs and design goals.

Component Two Analysis

Idle Wheel Leg:

By: Britney Ky, Omar Ramos Escoto

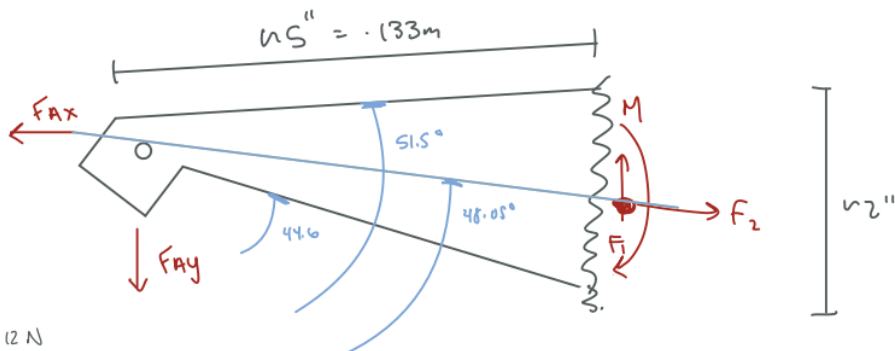


Because the primary purpose of the chassis and underside components are to house multiple wheels and hardware, their designs were guided primarily by the spacing specifications required by our FBDs. Thus, the remaining component with more design leeway is the leg component that attaches the rightmost idle wheel to the chassis. We identified this member as a component with a similar loading scenario to project one and thus an ideal candidate to mass optimize. We decided to begin with connecting the chassis to the side wheel with a simple beam, but the loading scenario inevitably introduced bending. Therefore, a wider base that merged to a smaller point was used to trace the stress patterns seen in bending members. We then leveraged Fusion 360's shape optimization software to study load path criticality, which confirmed our intuition of the stress distribution across the member, indicating that the material at the edges was most critical for the loading scenario and that it would be most ideal to reduce bending by spreading mass outwards from the original centroid.

As mentioned in the transmission analysis section, we used a pin and bearings as the right idle wheel. Bearings are press-fit into the PLA, while the pin is able to freely rotate about the bearing axis. The leg is attached to the chassis to the left of the drive wheel, minimizing any deflection experienced by this arm. We used tightened bolts to attach the leg to the chassis, which allows frictional load transfer, minimizing force multiplier errors. Only two bolts are needed to fully define the vertical position and orientation of the part; more could lead to error amplifiers as a result of being overconstrained.

BOTEA & Inverse Analysis:

The leg is modeled as a cantilever beam. Analysis shows that the beam would fail due to bending but spreading mass from the centroid increases its moment of inertia, improving resistance against bending moments. Thus, for our final design, we ran a shape optimization study to remove material in the center of the leg while maintaining a factor of safety of three.



$$F_A = 12 \text{ N}$$

$$F_{Ax} = 12 \cos(48.05^\circ) = 8.023 \text{ N}$$

$$F_{Ay} = 12 \sin(48.05^\circ) = 8.9247 \text{ N}$$

In bending :

$$\sigma = \frac{Sy}{FoS} = \frac{M \cdot y}{I}$$

$$\frac{(F_{Ay})(.127 \text{ m}) \left(\frac{h}{2}\right)}{\frac{1}{12} b h^3} = \frac{Sy}{FoS}$$

$$\frac{6(F_{Ay})(.127 \text{ m})}{b \cdot h^2} = \frac{Sy}{FoS}$$

$$\frac{6(8.9247)(.127)(\frac{h}{2})}{Sy} = bh^2$$

$$2.720 \times 10^{-7} \text{ m}^3 = bh^2$$

if $b=h \rightarrow .00647 \text{ m}$
 $\frac{\square h}{b} = .647 \text{ cm}$
 $= .254 \text{ "}$



considering I of an I-beam with no welding

$$I = 2 \left[\frac{1}{12} b t^3 + \left(\frac{h}{2} - \frac{t}{2} \right)^2 b t \right]$$

$$I = 2 \left[\frac{bt^3}{12} + \frac{(h-t)^4}{4} (bt) \right]$$

$$= \frac{bt^3}{6} + \frac{(h-t)^4 bt}{2} = \frac{bt^3 + 3(h-t)^4 bt}{6}$$

$$\frac{Sy}{FoS} = \frac{F_A \cdot L \cdot b \cdot h}{bt^3 + 3(h-t)^4 bt} \quad , \quad \text{if } b \frac{\square}{h} \quad b=h \quad \frac{F_A (1)(3)(1)(FoS)}{Sy} = \cancel{bt^3 + 3(h-t)^4 bt}$$

Smaller dimensions
than $I = \frac{1}{12} b h^3$

$$b=h = .00522 \text{ m} \\ = .522 \text{ cm} \\ = .20 \text{ "}$$

$$\Sigma F_x : F_{Ax} = F_2 = 8.023 \text{ N}$$

$$\Sigma F_y : F_{Ay} = F_1 = 8.9247 \text{ N}$$

$$\Sigma M_o : M = F_{Ay}(5") \\ = (8.9247)(.133 \text{ m}) \\ = 1.1861$$

In tension :

$$\bar{O}_S = \frac{F_{Ax}}{A} = \frac{Sy}{FoS}$$

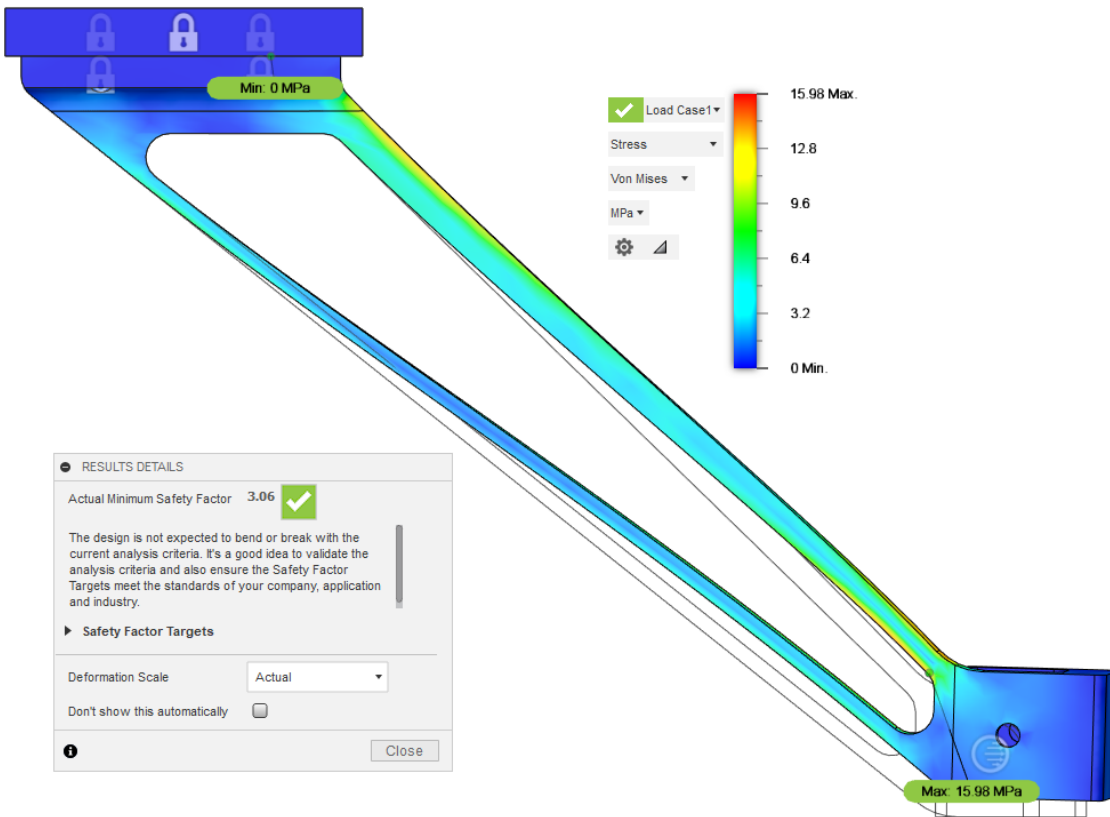
$$\frac{F_{Ax} \cdot FoS}{Sy} = A$$

$$\frac{(8.023)(2)}{50 \times 10^6} = A$$

$$A = 3.21 \times 10^{-7} \text{ m}^2$$

$a = 5.66 \times 10^{-4} \text{ m}$
 $\frac{\square}{b} I_a, \quad = .056 \text{ cm}$
 $= .022 \text{ "}$

FEA Analysis:



Constraints and Loading:

FEA analysis was conducted for stress and deformation. To simulate interaction with the wall of the chassis where components would interface, we generated contacts between the surfaces. We also used fixed bolt constraints in the holes to simulate how the part would interface with hardware as done in the FEA for the cantilever arm component. We applied a 12N load on the holes for the wheel shaft in the direction normal to the lip of the I-beam as described in our FBDs. Bearing loads were used to simulate the parabolic distribution of force from the shaft of the wheel. This scenario would mimic the anticipated behavior; the part seeks to rotate counterclockwise about its top left end but is constrained by the pin and contact with the wall of the chassis.

FEA Analysis:

As anticipated, uneven stress patterns indicate that a bending moment is occurring. The FEA corroborates the shape optimization study as we anticipated a factor of safety of 3. When mounted on the I-beam, the leg displays the shown deflection pattern, validating our FBDs, shape optimization study, and simulation results.